International Journal of Engineering Trends and Technology Volume 69 Issue 3, 1-6, March 2021
ISSN: 2231 – 5381 /doi:10.14445/22315381/IJETT-V69I3P201 © 2021 Seventh Sense Research Group®

Analysis of Subthreshold Characteristics for Top and Bottom Flat-band Voltages of Junction less Double Gate MOSFET

Hakkee Jung[#1]
[#]*Department of Electronic Engineering, Kunsan National University, Gunsan 54150, Korea*
[1]hkjung@kunsan.ac.kr

***Abstract** - The subthreshold characteristics are analyzed for the difference of the top and bottom flat-band voltage and dielectric constant of the junctionless double gate (JLDG) MOSFET. The potential distribution model of the asymmetric JLDG MOSFET is presented, and short-channel effects such as the degradation of subthreshold swing, the threshold voltage shift, drain induced barrier lowering (DIBL), and on-off current ratio are analyzed according to the flat-band voltage and the dielectric constant. As a result, the threshold voltage and on-off current ratio increase when the difference of the top and bottom flat-band voltage increases, but the subthreshold swing decreases. The DIBL is not affected by the flat-band voltage difference. As the constant dielectric increases, the threshold voltage and on-off current ratio increase, but DIBL and subthreshold swing decrease. In the case of the dielectric constant of 3.9, when the difference of the flat-band voltage increases from* V_{fbb}*-*V_{fbf}*=-0.5 V to* V_{fbb}*-*V_{fbf}*=0.5 V, the threshold voltage increases by 0.5 V, while the on-off current ratio increases by about* 10^3*. However, the increasing rate of the threshold voltage remains unchanged, and the on-off current ratio increases by about* 10^6 *when the dielectric constant is 25.*

Keywords — *Threshold voltage, Subthreshold swing, DIBL, On-off current, Flat-band voltage, Dielectric constant*

I. INTRODUCTION

The decrease in the size of transistors is seen as the most competitive in the semiconductor industry. Therefore, major semiconductor companies are manufacturing transistor structures in three dimensions to improve the integration density of integrated circuits. Representative three-dimensional transistors are FinFETs, double-gate MOSFETs, cylindrical MOSFETs, etc. [1-3]. However, due to the limitation of the development of doping technology caused by the size reduction, a junctionless MOSFET using the same doping concentration and type between the source/drain and the channel was developed rather than the junction-based transistor using a pn junction [4-6]. Unlike junction-based MOSFETs that operate in inverted mode, the junctionless MOSFET operates in accumulation mode. That is, the junctionless MOSFET depletes the channel in the subthreshold region, but it passes over the partial depletion region when the gate voltage increases and reaches the threshold voltage and enters into the accumulation mode when the gate voltage exceeds the flat-band voltage [7-9]. Therefore, the flat-band voltage defined by the difference between the work function of the gate metal and the silicon used as the channel becomes an important factor in determining the on-off state of the junctionless MOSFET. The junctionless MOSFETs have the advantage of being easier to process than the junction-based MOSFETs, enabling the fabrication of finer transistors. However, even a junctionless MOSFET cannot completely eliminate the short channel effects (SCEs) such as the degradation of subthreshold swing, lower on-off current ratio, larger drain induced barrier lowering (DIBL), and threshold voltage shift. Therefore, research is being conducted to use high-*k* materials as gate oxides to reduce such short channel effects [10-12]. When the high-*k* material is used as the oxide film, the oxide film can be made thicker than SiO_2, thereby reducing a phenomenon such as a gate parasitic current [13-15]. As such, the characteristics of the oxide film will directly affect the short channel effect. In this paper, the short channel effects of the junctionless double-gate (JLDG) MOSFET are analyzed using the high-*k* gate oxide according to the difference of the top and bottom flat-band voltage. In particular, by analyzing the short channel effect for the asymmetric JLDG MOSFETs with the different top and bottom flat-band voltages, the conditions having the optimum subthreshold characteristics will be presented.

Shin et al. discussed the variation of subthreshold current characteristics with respect to the variation of flat-band voltage and oxide thickness for junction-based double-gate MOSFETs with symmetric or asymmetric structures [16]. Abebe et al. analyzed the current-voltage characteristics assuming a flat-band voltage of zero with a hyperbolic potential distribution function [17]. In this paper, Ding's model, which induced potential distribution for asymmetric junction-based double gate MOSFET using Poisson's equation, is modified to apply to the JLDG structure [18]. Using the potential distribution, the subthreshold swing, threshold voltage, DIBL, and on-off current ratio are observed for the variation of the flat-band voltage. Particularly, the change of the short channel effect is observed when SiO_2 (k=3.9) and HfO/ZrO_2 (k=25) are used as gate oxide films.

This is an open access article under the CC BY-NC-ND license (http://creativecommons.org/licenses/by-nc-nd/4.0/)

II. ANALYSIS OF SHORT CHANNEL EFFECTS FOR THE ASYMMETRIC JLDG MOSFET

A. Potential distribution of the asymmetric JLDG MOSFET

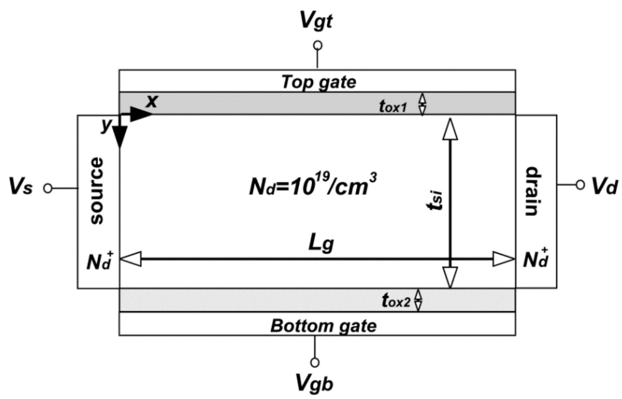

Fig. 1 Schematic cross-sectional diagram of the asymmetric junctionless double gate (JLDG) MOSFET

Figure 1 shows a schematic structure of the asymmetric JLDG MOSFET used in this paper. The source and drain are heavily doped with $n^{+,}$ and the channel is doped with N_d=10^{19} /cm^3. The flat-band voltages are examined for the difference between the top and bottom flat-band voltages, V_{fbb}-V_{fbf}, of from -0.5 V to 0.5 V. The channel length L_g is fixed at 15 nm and the silicon thickness t_{si} at 10 nm. The t_{ox1} and t_{ox2} using 2 nm are the top and bottom gate oxide thickness, respectively. The asymmetric junction-based potential distribution function derived by Ding et al. is modified to meet the boundary condition of the junctionless MOSFET as the followings ;

$$\phi(x,y) = V_s + \frac{V_d x}{L_g} + \sum_{n=1}^{\infty} A_n(y) \sin\frac{n\pi x}{L_g}, \qquad (1)$$

$$A_n(y) = f(V_{fbf}, V_{fbb}, C_{ox1}, C_{ox2})$$

where C_{ox1} and C_{ox2} are the top and bottom gate oxide capacitances represented by $\varepsilon_{ox1}/t_{ox1}$ and $\varepsilon_{ox2}/t_{ox2}$ V_d and V_s are the drain and source voltages, and V_{fbf} and V_{fbb} indicate the top and bottom flat-band voltages, respectively. The dielectric constants of 3.9 and 25 for ε_{ox1} and ε_{ox2} are used. As shown in the previously published paper [19, 20], the $A_n(y)$ is the function of V_{fbf} and V_{fbb} to indicate the top and bottom flat-band voltages, and ε_{ox1} and ε_{ox2} to describe the dielectric constants of the top and bottom gate oxides.

The potential distributions are changed with the flat-band voltages and dielectric constants of the top and bottom gates,

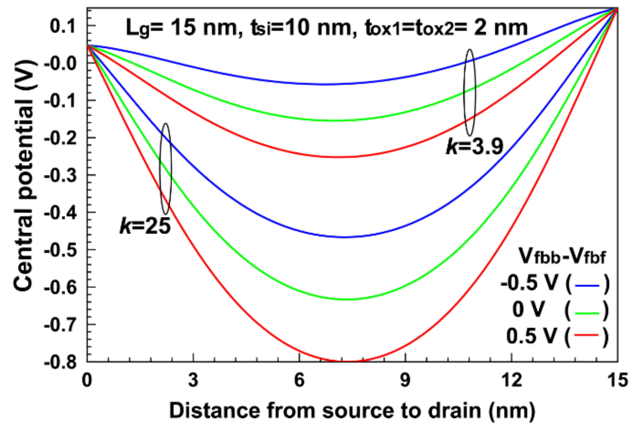

Fig. 2 Central potential distributions along from source to drain with the difference of top and bottom flat-band voltages and dielectric constants as parameters

So subthreshold characteristics are affected by those. Figure 2 shows the central potential distribution obtained with the dielectric constants and the difference of the top and bottom flat-band voltages as parameters, using the potential distribution function obtained using Eq. (1). As the difference between the top and bottom flat-band voltages V_{fbf} -V_{fbb} increases, the central potential distribution decreases. Decreasing the potential distribution can predict an increase in the threshold voltage. In addition, it can be seen that the potential distribution decreases significantly as the dielectric constant of the top and bottom gate oxide films increases.

Thus, it can be seen that the potential distribution in the central axis, which is the conduction path of the symmetric JLDG MOSFET, is greatly changed by the flat-band voltage and the dielectric constant of the gate oxide film. The change in the potential distribution with respect to the change in the flat-band voltage will affect the threshold voltage. This change in the threshold voltage will directly affect the threshold voltage shift and the on-off current ratio. Since the change in the potential distribution affects the short channel effects, the short channel effect will be analyzed, using the potential distribution function of Eq. (1) in this paper.

B. Analysis of subthreshold swing

In the asymmetric structure, the subthreshold swing represents the change of the top gate voltage with respect to the drain current change in the subthreshold region, and if the electron density constituting the drain current can be approximated by Boltzmann distribution like $n \approx N_d e^{q\phi_{min}/kT}$, the subthreshold swing can be expressed by the following Eq. (2).

$$SS = \frac{\partial V_{gt}}{\partial \log I_{ds}} = \ln(10)\left(\frac{kT}{q}\right)\left(\frac{\partial \phi_{\min}}{\partial V_{gs}}\right)^{-1} \qquad (2)$$

At this time, to obtain the $\phi_{\min}$, find x=$x_{\min}$ satisfying $\partial\phi(x,t_{si}/2)/\partial x$, and substitute $x_{\min}$ into Eq. (1). Here, in the case of the symmetrical JLDG MOSFET, most electrons move through the center of the channel, but in the case of the asymmetric JLDG MOSFET, the conduction path will change according to the top and bottom flat-band voltages and gate voltages. Therefore, the effective conduction path y_{eff} is derived using the following equation [21].

$$y_{eff} = \int_0^{t_{si}} y n(x_{\min}, y) dy \Big/ \int_0^{t_{si}} n(x_{\min}, y) dy \qquad (3)$$

The subthreshold swing can be obtained by the Eq. (2), using the $\phi_{\min}$ obtained by substituting the $x_{\min}$ and y_{eff} into Eq (1).

The change in the conduction path obtained using Eq. (3) is shown in Fig. 3 according to the difference of the flat-band voltages. As shown in Fig. 3, the y_{eff} value changes as the difference of flat-band voltage changes, indicating that the subthreshold swing is affected by the flat-band voltage. As shown in Fig. 3, the conduction path y_{eff} moves to the bottom gate in the region where the relation of the top and bottom flat-band voltages are $V_{\mathrm{fbb}} < V_{\mathrm{fbf}}$. It moves to the midpoint at $V_{\mathrm{fbb}} = V_{\mathrm{fbf}}$, and to the top gate in the region of $V_{\mathrm{fbb}} > V_{\mathrm{fbf}}$. That is, since the change of the drain current with respect to the top gate voltage is defined as the subthreshold swing as shown in Eq. (2), it can be expected that the control ability of the conduction phenomenon by the top gate voltage is further increased and the subthreshold swing will decrease when the conduction path moves to the top gate.

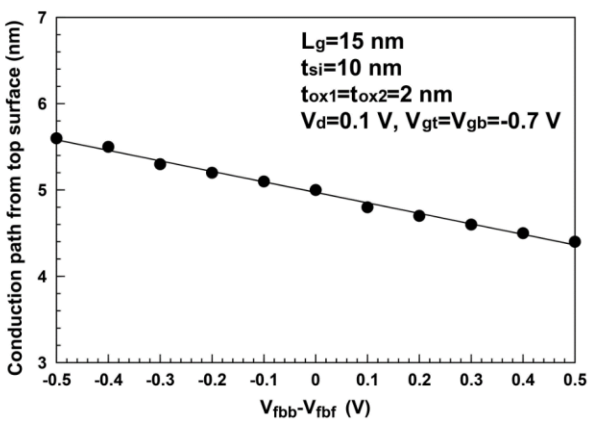

Fig. 3. Conduction path from the top surface for the difference of top and bottom flat-band voltages

C. Threshold voltage and DIBL

In the conventional MOSFET structure, the threshold voltage is proportional to the flat-band voltage. Therefore, the difference of the top and bottom flat-band voltages in the asymmetric double-gate MOSFET will directly affect the threshold voltage. There are various ways to calculate the threshold voltage, but in this paper, the SD (Second-Derivative) method is used, which finds the minimum value by quadratic differentiating of the drain current-gate voltage relationship [22]. This method is conceived from the change of drain current rapidly increasing at threshold voltage in SPICE LEVEL 1 model, using to calculate the change of transconductance with respect to the gate voltage. In order to use this method, the drain current-gate voltage relationship is derived using the following Eq. (4).

$$I_d = \frac{q n_i \mu_n W k T \left\{1 - \exp\left(\frac{-qV_d}{kT}\right)\right\}}{\int_0^{L_g} \frac{1}{\int_0^{t_{si}} \exp\left(\frac{-q\phi(x,y)}{kT}\right) dy} dx} \qquad (4)$$

As shown in Fig. 2, the minimum value of the potential distribution function decreases as V_{fbb}-V_{fbf} increases in the subthreshold region. That is, the amount of current flowing below the threshold voltage will also decrease, thereby increasing the threshold voltage. In addition, it can be predicted that as the dielectric constant of the oxide increases, the potential distribution decreases, thereby increasing the threshold voltage. In this paper, d^2I_d/dV_g^2 is obtained from the current-voltage relationship obtained using Eq. (4) to find the threshold voltage at the inflection point from the SD method. Figure 4 shows the current-voltage relation obtained from Eq. (4) and the threshold voltage obtained by using the SD method with the difference of the flat-band voltage as a parameter in the case of the dielectric constant of 3.9. It can be observed that the threshold voltage changes according to the difference in the top and bottom flat-band voltages.

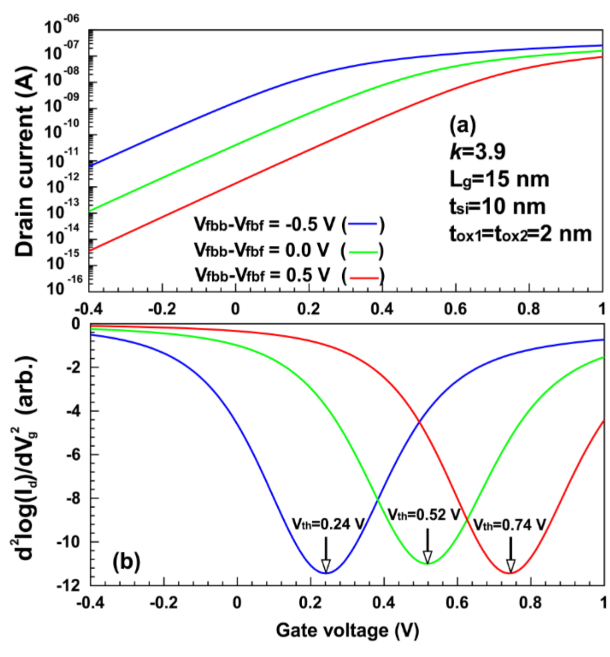

Fig. 4 (a) Drain current vs. gate voltage curve and (b) extraction of the threshold voltage from SD method with the difference of the top and bottom flat-band voltages as a parameter in the case of *k*=3.9

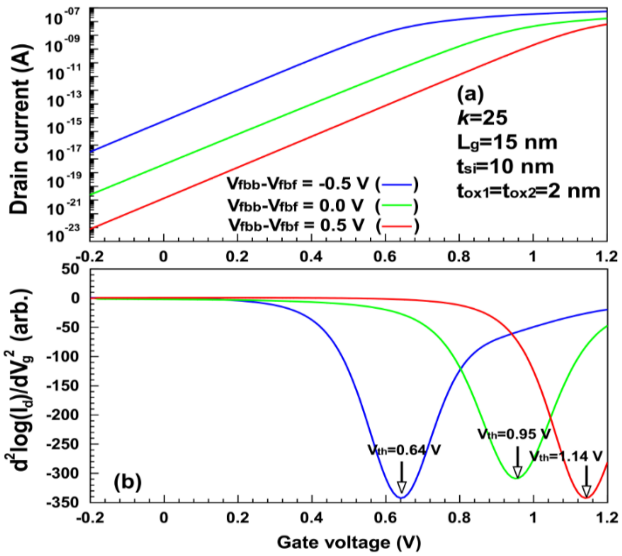

Fig. 5 (a) Drain current vs. gate voltage curve and (b) extraction of the threshold voltage from SD method with the difference of the top and bottom flat-band voltages as a parameter in the case of *k*=25

When the dielectric constant of the gate oxide film is increased to 25, the current-voltage characteristics and the threshold voltages according to the flat-band voltage difference are shown in Fig. 5. It can be seen from the comparison with Fig. 4 that the currents drop more rapidly in the subthreshold region when the constant dielectric increases. From this, it can be expected that the subthreshold swing reduces with increasing the dielectric constant of the gate oxide. It has also been observed that the threshold voltage derived from the SD method is increasing with the dielectric constant.

The DIBL is a measure to indicate the effect of drain voltage on the threshold voltage. It is demonstrated in a previously published paper that the DIBL is linearly proportional to oxide thickness [23, 24]. The DIBL will be observed for the change of dielectric constant and the difference of flat-band voltages of the top and bottom gate oxide layers using the following Eq. (5).

$$DIBL = V_{th}(V_d = 0.1V) - V_{th}(V_d = 1.1V) \tag{5}$$

D. Analysis of on-off current ratio

The drain current at the threshold voltage is defined as the on-current I_{on} and the drain current at $V_{gt}=V_{gb}=0$ V as the off-current I_{off}, and then the on-off current ratio I_{on}/I_{off} is obtained. A larger on-off current ratio will reduce parasitic currents [25, 26]. The on-off current ratio increases as the threshold voltage increases, as shown in Fig. 4 and Fig. 5. Therefore, the increase in the static power consumption that may occur due to the increase in the threshold voltage may be offset by the decrease in the parasitic current caused by the increase of the on-off current ratio [27]. However, the increase in the threshold voltage is about a tenth of a volt, whereas the on-off current ratio increases by several orders of magnitude, so the increase in the on-off current ratio will have a great effect on the reduction of parasitic current. As described above, as V_{fbb}-V_{fbf} increases, the threshold voltage will increase, so the on-off current ratio will also increase. In addition, as the dielectric constant of the oxide increases, the threshold voltage increases, so the on-off current ratio will also increase. The on-off current ratio is related not only to the threshold voltage but also to the subthreshold swing as the following Eq. (6) and Eq. (7).

$$SS = \frac{dV_{gt}}{d\log(I_d)} = \frac{V_{th} - 0}{\log(I_{on}) - \log(I_{off})} = \frac{V_{th}}{\log(I_{on}/I_{off})} \tag{6}$$

$$I_{on}/I_{off} = 10^{\frac{V_{th}}{SS}} \tag{7}$$

Since the threshold voltage and the subthreshold swing will be greatly affected by changes in the flat-band voltage and the dielectric constant, the on-off current ratio will also be affected by these parameters. Table 1 shows the relationship between the threshold voltage and the on-off current ratio obtained in Fig. 4 and Fig. 5. As can be seen from Table 1, the threshold voltage increases by 0.5 V while the on-off current ratio increases by about 10^3 times when the value of V_{fbb}-V_{fbf} increases from -0.5 V to 0.5 V in the case of the dielectric constant of 3.9. Also, it can be observed that the on-current is hardly affected by the change of V_{fbb}-V_{fbf}, but the off-current is greatly affected, and the on-off current ratio is determined by the off-current. When the dielectric constant of the gate oxide film is increased from 3.9 to 25, the change in the threshold voltage according to the flat-band voltage difference V_{fbb}-V_{fbf} from -0.5 V to 0.5 V is constant at 0.5 V, but one of the on-off current ratios is increased from 10^5 to 10^8 times as shown in Table 1.

TABLE I. THRESHOLD VOLTAGE AND ON-OFF CURRENT RATIOS OBTAINED IN FIGS. 4 AND 5

SCE	Dielectric constant	V_{fbb}-V_{fbf} (V)		
		-0.5	0	0.5
V_{th} (V)	3.9	0.24	0.52	0.74
	25	0.64	0.95	1.14
I_{off} (A)	3.9	1.74×10^{-9}	4.05×10^{-11}	1.39×10^{-12}
	25	5.71×10^{-21}	3.90×10^{-24}	1.35×10^{-26}
I_{on} (A)	3.9	2.37×10^{-8}	2.40×10^{-8}	2.37×10^{-8}
	25	3.04×10^{-14}	2.51×10^{-14}	3.04×10^{-14}
I_{on}/I_{off}	3.9	1.30×10^{1}	5.90×10^{2}	1.70×10^{4}
	25	5.30×10^{6}	6.40×10^{9}	2.30×10^{12}

Using this method, changes in subthreshold swing, threshold voltage, DIBL, and the on-off current ratio will be analyzed according to the difference in the flat-band voltage.

III. THE SHORT CHANNEL EFFECTS OF THE ASYMMETRIC JLDG MOSFET

Fig. 6 Short channel effects for the difference between the

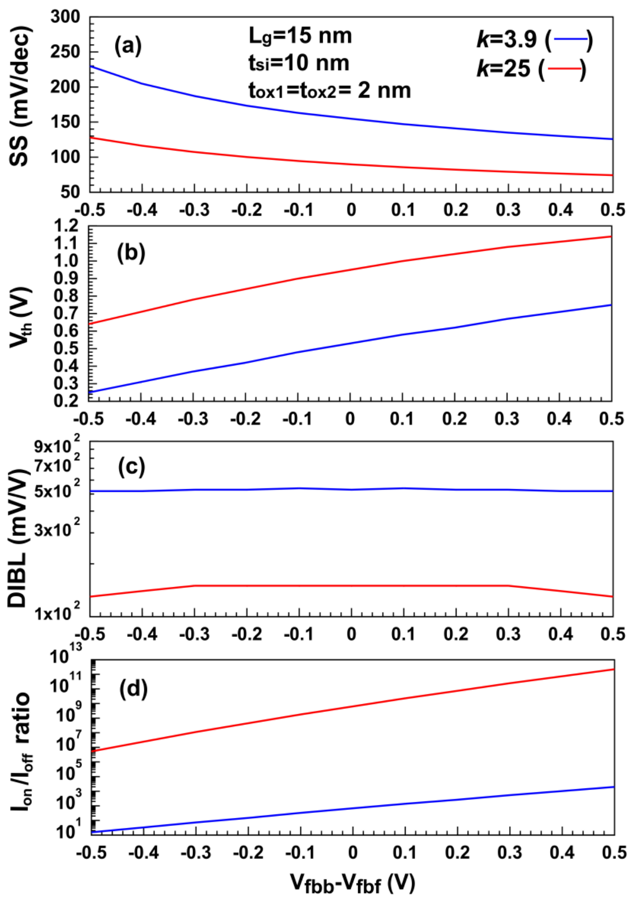

top and bottom flat-band voltages with dielectric constant as a parameter. (a) subthreshold swing (b) threshold voltage (c) drain induced barrier lowering (d) on-off current ratio

Since the validity of Eq. (1) is demonstrated in the previous papers [18,19], the short channel effects will be analyzed, such as the subthreshold swing, threshold voltage, and DIBL and on-off current ratio derived, using Eq. (1). Using the potential distribution of Eq. (1), the short channel effects obtained for the differences of top and bottom flat-band voltage with the dielectric constant of the gate oxide film as a parameter are shown in Fig. 6.

Figure 6(a) shows the change in the subthreshold swing with respect to the flat-band voltage difference of the top and bottom gates. As the flat-band voltage difference increases, the subthreshold swing decreases. As shown in Fig. 3, as the flat-band voltage difference increases, the conduction path will move toward the top gate direction so that the control of the gate voltage will be improved, and the subthreshold swing will decrease. Therefore, in order to reduce the subthreshold swing, the corresponding gate metal that can make the flat-band voltage of the bottom gate larger than the flat-band voltage of the top gate should be used for the top and bottom gates. In addition, if a material with a high dielectric constant is used as the gate oxide film, the subthreshold swing can be further reduced, as shown in Fig. 6(a). In particular, since the reduction rate of the subthreshold swing due to the flat-band voltage difference is not so large in the range of $V_{fbb}>V_{fbf}$, the use of a high-*k* gate oxide film in this range will help to improve the subthreshold swing characteristics.

Figure 6(b) shows the change of threshold voltage with respect to the difference of top and bottom flat-band voltage. It can be seen that the threshold voltage increases in the $V_{fbb}>V_{fbf}$ region rather than the symmetric structure ($V_{fbb}=V_{fbf}$) but decreases in the $V_{fbb}<V_{fbf}$ region. In particular, the threshold voltage is further increased when a high-*k* material is used as the gate oxide film. This is due to the reduction of the potential distribution, as illustrated in Fig. 2. An increase in the threshold voltage will result in an increase in static power consumption. However, if the parasitic current in the subthreshold region is reduced, the increase in static power consumption due to the increase in the threshold voltage can be sufficiently offset. As can be seen in Fig. 4 and Fig. 5, it can be observed that the current also decreases in the subthreshold region as the threshold voltage increases.

Figure 6(c) shows the variation in the DIBL for the difference of the flat-band voltages, and it can be seen that the DIBL is not affected by the difference of flat-band voltages. It was also observed that the DIBL decreases when the high-*k* oxide film is used.

Figure 6(d) shows the variation of the on-off current ratio for the difference of the flat-band voltages, and It is observed that the on-off current ratio in the region of $V_{fbb}<V_{fbf}$ decreases more than in $V_{fbb}=V_{fbf}$, but increases in $V_{fbb}>V_{fbf}$ region. In addition, the use of a high-*k* material in the oxide film increases the on-off current ratio. As can be seen from Eq. (6), the on-off current ratio is proportional to the threshold voltage and inversely proportional to the subthreshold swing. As can be seen in Fig. 6, as the flat-band voltage difference increase, the threshold voltage increases, and the subthreshold swing decreases, so the logarithm of the on-off current ratio is linearly proportional to the flat-band voltage difference. As can be seen from Eq. (7), the threshold voltage increases, and the subthreshold swing decreases when the high-*k* oxide film is used, thus increasing the on-off current. As described in Table 1, the threshold voltage increases by about 0.5 V regardless of the dielectric constant of the oxide film when V_{fbb}-V_{fbf} increases from -0.5 to 0.5 V, but the on-off current ratio increases by 10^3 times when k=3.9, while an increase of about 10^6 times at k=25 can be observed in Fig. 6(d) when V_{fbb}-V_{fbf} increases from -0.5 to 0.5 V.

IV. CONCLUSIONS

In this paper, the short channel effects of the asymmetric JLDG MOSFET were observed by the difference of the top and bottom flat-band voltages and dielectric constants of an oxide film. For this purpose, a potential analytical distribution obtained using the Poisson's equation is used, and the threshold voltage, the subthreshold swing, the DIBL, and the on-off current ratio were analyzed, using the change of potential distribution and the conduction path corresponding to the difference of the flat-band voltages and the change of dielectric constants of the oxide film. As a result, it was observed that the threshold voltage and the on-off current ratio were greatly affected by the potential distribution, and the subthreshold swing was greatly affected by the conduction path. As the flat-band voltage difference increases, the subthreshold swing decreases, but the threshold voltage and the on-off current ratio increase. In the case of the DIBL, the results were independent of the flat-band voltage. If the dielectric constant of the top and bottom oxide films increases, the subthreshold swing and DIBL decrease, but the threshold voltage and on-off current ratio increase. As the short channel effects may be improved or worsened according to the flat-band voltage difference between the top and bottom and the dielectric constant of the oxide layer, the JLDG MOSFET may be designed by adjusting the difference between the top and bottom flat-band voltages so that the short channel effects can be improved, depending on the use of the device.

REFERENCE

[1] R. U. Ahmed, R. Saha, M. R. Adnan, and ShowmikSingha, Impact of Channel Length Variation on Short Channel Effect Parameters of Two Different GAA Nanowire Transistor Structure, International Journal of Engineering Trends and Technology, 67(8) (2019) 83-86.

[2] V. Kumar, R. Gupta, R. P. P. Singh, and R. Vaid, Performance Analysis of Double Gate n-FinFET Using High-k Dielectric Materials, International Journal of Innovative Research in Science, Engineering and Technology, 5(7) (2016) 13242-13249.

[3] K. Liu, and L. Yang, Investigation on Fin and Gate Line Edge Roughness Effects for Sub-22 nm Inversion-Mode and Junctionless FinFETs, International Journal of Engineering Trends and Technology, 40(2) (2016) 72-76.

[4] L. Chen, M. Yeh, Y. Lin, K. Lin, M. Wu, V. Thirunavukkarasu and Y. Wu, The Physical analysis on the electrical junction of junctionless FET, AIP ADVANCES, 7(2) (2017) 025301.

[5] G. L. Priya and N. B. Balamurugan, New dual material double gate junctionless tunnel FET: Subthreshold modeling and simulation, International Journal of Electronics and Communications, 99 (2019) 130-138.

[6] Q. Xie, Z. Wang, and Y. Taur, Analysis of Short-Channel Effects in Junctionless DG MOSFETs, IEEE Trans. Electron Devices, 64(8) (2017) 3511-3514.

[7] Raksharam, and A. K. Dutta, A unified analytical drain current model for Double-Gate Junctionless Field-Effect Transistors including short channel effects, Solid-State Electronics, 130 (2017) 33-40.

[8] J. P. Colinge, A. Kranti, R. Yan, C. W. Lee, I. Ferain, R. Yu, N. D. Akhavan, and P. Razavi, Junctionless Nanowire Transistor (JNT): Properties and design guidelines, Solid-State Electronics, 65-66 (2011) 33-37.

[9] S. K. Yadav, and R. Singh, Analysis and Comprehensive study of Junction-less transistor, Intl. J. Eng. Sci. Adv. Research, 4(2) (2018) 103-120.

[10] J. Ajayan, D. Nirmal, P. Prajoon and J. C. Pravin, Analysis of nanometer-scale InGaAs/InAs/InGaAs composite channel MOSFETs using high-k dielectric for high-speed applications, International Journal of Electronics and Communications, 79 (2017) 151-157.

[11] A. Balhara and D. Punia, Design and Analysis of Double Gate MOSFET Devices using High-k Dielectric, International Journal of Electrical Engineering, 7(1) (2014) 53-60.

[12] Nirmal, V. Kumar, P. C. Samuel, Shruthi, D. M. Thomas and M. Kumar, Analysis of Dual Gate MOSFETs Using High k Dielectrics, in Proc. 2011 3rd International Conference on Electronics Computer Technology, (2011) 22-25.

[13] P.S. Raja, R. J. Daniel, Effect of gate dielectric on the threshold voltage of nanoscale MOSFETs, International Journal of Engineering Research and Development, 5(3) (2012) 93-104.

[14] Sakshi, S. Dhariwal and A. Singh Analyzing the effect of gate dielectric on the leakage currents, MATEC Web of Conferences, 57 (2016) 01028.

[15] M. Karbalaei, D. Dideban, and H. Heidari, Impact of high-k gate dielectric with different angles of coverage on the electric characteristics of gate-all-around field-effect transistor: A simulation study, Results in Physics, 16 (2020) 102823.

[16] Y. H. Shin, S. Weon, D. Hong and I. Yun, Analytical Model for Junctionless Double-Gate FET in Subthreshold Region, IEEE Trans. Electron Devices, 64(4) (2017) 1433-1440.

[17] H. Abebe, E. Cumberbatch, H. Morris, V. Tyree, T. Numata, and S. Uno, Symmetric and Asymmetric Double Gate MOSFET Modeling, J. of Semiconductor Technology and Science, 9(4) (2009) 225-232.

[18] Z. Ding, G. Hu, J. Gu, R. Liu, L. Wang, and T. Tang, An analytical model for channel potential and subthreshold swing of the symmetric and asymmetric double-gate MOSFETs, Microelectronics J., 42(3) (2011) 515-519.

[19] H. Jung, Top and Bottom Gate Oxide Thickness Dependent Subthreshold Swing in Asymmetric Junctionless Double Gate MOSFET, International Journal of Electrical and Electronic Engineering & Telecommunications, 8(5) (2019) 292-296.

[20] H. Jung, Analysis of subthreshold swing in junctionless double-gate MOSFET using stacked high-*k* gate oxide, International Journal of Electrical and Computer Engineering, 11(1) (2021) 240-248.

[21] P. K. Tiwari, C. R. Panda, A. Agarwal, P. Sharma, and S. Jit, Analytical Modeling of Effective Conduction Path Effect(ECPE) on the Subthreshold Swing of DG-MOSFETs, in Proc. of the 2009 Spanish Conference on Electron Devices, (2009) 136-139.

[22] A. Ortiz-Conde, F. J. Carcia-Sanchez, J. Muci, A. T. Barrios, J. J. Liou, and C. Ho, Revisiting MOSFET threshold voltage extraction methods, Microelectronics Reliability, 53(1) (2013) 90-104.

[23] S. Dimitrijev, Principles of Semiconductor Devices, 2nd ed. New York, NY: Oxford University Press, (2012) 453.

[24] H. Jung, SPICE Model of Drain Induced Barrier Lowering in Symmetric Junctionless Double Gate MOSFET, International Journal of GEOMATE, 16(55) (2019) 20-27.

[25] T. Kang, C. Hsu, H. Liu, F. Chien, and C. Lin, Effect of transistor behavior on off-state current in poly-Si junctionless nanowire thin-film transistor, Jpn. J. Appl. Phys., 59 (2020) 126503.

[26] P. K. Asthana, Y. Goswami, S. Basak, S. B. Rahi, and B. Ghosh, Improved performance of a junctionless tunnel field-effect transistor with a-Si and SiGe heterostructure for ultra low power applications, RSC Advances, 5(60) (2015) 48779-48785.

[27] J. Innocenti, L. Welter, F. Julien, L. Lopez, J. Sonzogni, S. Niel, A. Regnier, E. Paire, K. Labory, E. Denis, J. Portal, and P. Masson, Dynamic Power Reduction through Process and Design Optimizations on CMOS 80 nm Embedded Non-Volatile Memories Technology, in Proc. 2014 IEEE 57th international Midwest Symposium on Circuits and Systems (MWSCAS), College Station, TX, USA, (2014) 897-900.